Available online at www.sciencedirect.com

ScienceDirect

Energy Procedia 49 (2014) 530 – 537

Energy Procedia

SolarPACES 2013

Optical characterization and modeling of coatings intended as high temperature solar selective absorbers

A.Soum-Glaude[a,]*, I. Bousquet[b,c], M. Bichotte[a], S. Quoizola[b,c], L. Thomas[b,c], G. Flamant[a]

[a] *Laboratoire CNRS-PROMES, 7 rue du Four Solaire, 66120 Font-Romeu Odeillo, France*
[b] *Laboratoire CNRS-PROMES, Rambla de la Thermodynamique Tecnosud, 66100 Perpignan, France*
[c] *University of Perpignan Via Domitia (UPVD), 52 Av. Paul Alduy, 66100 Perpignan, France*

Abstract

SiCNH thin coatings synthesized by Plasma Enhanced Chemical Vapor Deposition (PECVD) are considered as high temperature ceramic materials for solar selective multilayer absorbers. As indicated by ellipsometry and spectrophotometry measurements, their optical characteristics make them suitable as solar absorbing and antireflective coatings in multilayer stacks and/or ceramic-metal composites (cermets). These measurements gave access to spectral values of complex refractive index $N = n + ik$, reflectance R and transmittance T of the coatings. R and T were also modeled from N, based on Fresnel equations, and a good agreement was found between simulated and measured reflectance in the visible region. A transfer matrix method was then applied to predict the optical response (R, T) of virtual multilayer stacks including SiCNH materials. W-SiCNH cermets were also considered as absorptive layers in these stacks and their refractive indices were calculated using Bruggeman effective medium approximation theory. Solar absorptance α_S and thermal emittance $\varepsilon(T)$ were estimated from simulated reflectance. Layer thicknesses and cermet composition were optimized using CODE software and a MATLAB in-house code, so as to maximize solar-heat conversion efficiency which relied on high α_S (up to 95%) and low ε (down to 6% at 500°C). The corresponding global yield which could be attained in typical Fresnel and central tower solar plants using these selective coatings was also calculated and compared to current technology.

Selection and peer review by the scientific conference committee of SolarPACES 2013 under responsibility of PSE AG.
Final manuscript published as received without editorial corrections.

Keywords: High temperature solar selective coatings; Optical modeling and characterization; Concentrated Solar Power

* Corresponding author. Tel.: +33-468-307-747; fax: +33-468-307-799.
E-mail address: Audrey.Soum-Glaude@promes.cnrs.fr

Selection and peer review by the scientific conference committee of SolarPACES 2013 under responsibility of PSE AG.
Final manuscript published as received without editorial corrections.
doi:10.1016/j.egypro.2014.03.057

1. Introduction

Concentrated Solar Power (CSP) technologies first convert concentrated solar radiation into heat before generating electricity through a thermodynamic process. One of the most important parts of a CSP plant is therefore the solar receiver, where the radiation-heat conversion occurs, and the generated heat is transferred to a heat transfer fluid (HTF). Solar receivers basically consist of stainless steel piping. As the latter absorbs and reflects solar light while emitting infrared radiation when heated under concentrated solar flux, a spectrally selective coating is usually deposited on the solar receiver. Such coatings associate several materials in multilayer stacks, comprising highly solar absorbing and antireflective layers (low VIS-NIR reflectance) and low-emissive metallic layers (high IR reflectance) to limit radiative emission and subsequent thermal losses. The most common absorber materials are metal-ceramic composites (cermets), e.g. Mo-Al_2O_3 [1], Mo-SiO_2 [2] or W-Al_2O_3 [3], arranged in double-layer absorbers with low and high metal volume fractions (LMVF/HMVF) [1-2]. Most commercialized selective coatings were developed for parabolic trough linear receivers working with synthetic oil HTF below 400°C. New generation CSP plants combine direct steam generation (DSG) or molten salt HTF with linear Fresnel reflectors or central towers to reach higher efficiencies at temperatures $\geq$ 500°C. New solar selective coatings able to withstand these higher temperatures must therefore be developed. Recently, transition metal oxides, nitrides, and oxynitrides such as (Ti,Al)(O,N) synthesized by plasma PVD deposition techniques were tested [4-5]. Expected selective properties are typically solar absorptance α_S > 90% and thermal emittance ε(700°C) < 40% (claimed goals for the National Renewable Energy Laboratory (NREL) in U.S. Department of Energy SunShot Initiative [6]).

SiCH films are also good candidates as ceramic materials in high temperature solar selective coatings. Indeed, these materials are widely used in mechanical and photovoltaic applications [7-10] for their high hardness and good thermal stability up to 650°C under air [8]. Their thermal annealing at T > 650°C only leads to higher solar absorption [9]. Moreover, TiSi-based optical stacks are considered for high-temperature selective absorbers [11] and Ti-SiCH coatings were previously used as mid-temperature selective coatings [12]. In this work, the potential of PECVD-grown SiCNH thin films as ceramic materials for high temperature solar selective coatings was investigated. High refractive index SiCNH layers are envisaged as matrices for high temperature solar absorbing cermets with tungsten (high melting point refractory metal) inclusions, in solar selective multilayer stacks. Low refractive index SiCNH could also be used as antireflective top-layer. For this purpose, high and low refractive index SiCNH thin films were grown by microwave PECVD from Ar/TMS/NH_3 mixtures (tetramethylsilane $Si(CH_3)_4$). Their complex refractive indices (n, k) were measured by ellipsometry and served as input data for the transfer matrix calculation of spectral reflectance and transmittance for single SiCNH layers, W-SiCNH cermets and multilayer stacks including these layers. Reflectance was also measured by spectrophotometry and compared to calculation. Solar absorptance and thermal emittance were derived from reflectance values.

2. Experimental details

A Plasma Enhanced Chemical Vapor Deposition (PECVD) reactor implemented with four microwave (2.45 GHz) coaxial sources was used to synthesize SiCNH thin coatings at 350°C. Reactive plasmas were generated from 1:4:5 mixtures of TMS (tetramethylsilane = $Si(CH_3)_4$) and NH_3 precursors diluted in argon. Coatings were grown on silicon (100) substrates. Complex refractive indices (n, k) of SiCNH layers in the 430 – 850 nm range were determined by spectroscopic ellipsometry, thanks to a Jobin Yvon MM-16 polarimetric ellipsometer at an incident angle of 76°. Results were fitted using the New Amorphous dispersion formula [13]. Spectral directional reflectance was also measured with a SOC-100 HDR spectrophotometer in the 400 – 1000 nm range at near normal incidence (10°).

3. Optical theory

3.1. Optical properties

Spectral reflectance, transmittance and absorptance at normal incidence were calculated for SiCNH single layers and potential multilayer stacks including such layers. For this purpose, a transfer matrix model using Fresnel

equations [14] was implemented in MATLAB software. Refractive indices of the constituting materials were required for this model. SiCNH refractive indices were measured by ellipsometry in the visible range and fitted by a new amorphous dispersion formula [13] to extrapolate in the IR range. In the case of multilayer stacks, metallic and W-SiCNH composite layers were considered as IR reflective and absorptive layers, respectively. Refractive index data for W were taken from the literature [15]. For W-SiCNH cermets, an effective refractive index was determined using Bruggeman Effective Medium Approximation (EMA) theory [16]. As in CSP plants most solar receivers to be selectively coated consist of stainless steel (SS) piping, SS substrates were considered for calculation. SS refractive indices were measured in the visible range by ellipsometry on a 316L stainless steel sample. These measurements were fitted with a Drude model to extrapolate (n,k) in the NIR-IR range.

Solar absorptance α_S and thermal emittance $\varepsilon(T)$ were deduced from calculated $A(\lambda) = 1 - R(\lambda)$ values integrated over wavelength and weighted by the solar spectrum (ASTM G173-03 Air Mass 1.5) and by the blackbody radiation spectrum, respectively. According to Kirchhoff's law of radiation, a material can emit any radiation it can absorb at a given wavelength and temperature; $A(\lambda_{IR})$ values are therefore representative of the emissive power of materials. Layer thicknesses of the different multilayer stacks were optimized so as to maximize the photothermal efficiency at a given concentration factor (C = 50 and 500) and temperature (T = 500°C). For this purpose, CODE software [17] and MATLAB multiobjective goal attainment algorithm [18] were implemented.

3.2. Thermo-optical and global efficiencies

Fig. 1 illustrates the energy balance for the solar receiver. Depending on its optical characteristics, the receiver converts only a portion α_S of the incident solar power P_{sol} into useful power P_u, which is transmitted to the heat transfer fluid (HTF). Some of the incident power is also wasted through thermal losses P_{loss}. The energy balance for the solar receiver is thus:

$$\alpha_S \cdot P_{sol} = P_u + P_{loss} \tag{1}$$

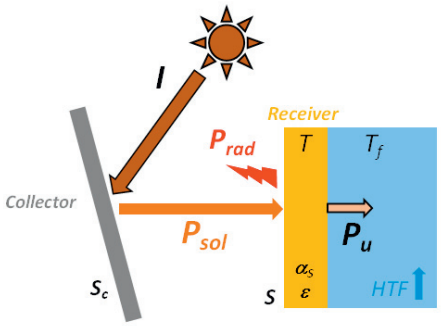

Fig.1. Energy balance for the solar receiver (see text for legend).

P_{sol} is given by (2). P_{sol} depends on the solar collector total surface S_C, the direct solar irradiation I and the collector optical efficiency η_{opt}, which takes into account the collector reflectivity (ρ was chosen as 95%), the intercept factor, *i.e.* the fraction of reflected rays that actually reach the solar receiver (γ was chosen as 95%).

$$P_{sol} = S_C \cdot I \cdot \eta_{opt} \tag{2}$$

Thermal losses P_{loss} occur by radiative (infrared emission), conductive (receiver-fluid heat exchange) and convective (ambient air) processes. In this case, we neglected convective and conductive losses ($T_{receiver} = T_{HTF}$). We

only considered radiative losses P_{rad}, given by Stefan–Boltzmann law (3) at the receiver temperature T, depending on its thermal emittance ε and area S (T_0 is the ambient temperature).

$$P_{loss} \approx P_{rad} = \varepsilon(T) \cdot \sigma\left(T^4 - T_0^4\right) \cdot S \tag{3}$$

The thermo-optical efficiency, or photothermal yield $\eta_{photothermal}$, represents the radiation-heat conversion efficiency and is given by (4), where C is the concentration factor of the system ($C = S_C / S$):

$$\eta_{photothermal} = \frac{P_u}{P_{sol}} = \alpha_S - \frac{\varepsilon(T) \cdot \sigma\left(T^4 - T_0^4\right)}{C \cdot I \cdot \eta_{opt}} \tag{4}$$

A solar power plant further converts the produced heat into mechanical work in a steam or air turbine. The maximum thermodynamic efficiency is given by Carnot's yield:

$$\eta_{Carnot} = 1 - \frac{T_0}{T} \tag{5}$$

Common thermodynamic cycles achieve approx. 75% of Carnot efficiency, therefore a $0.75 * \eta_{Carnot}$ thermodynamic efficiency was considered for the calculation of global efficiency η_{global}, which is the product of photothermal and thermodynamic yields.

4. Results

4.1. Optical characteristics and aging of SiCNH coatings

SiCNH materials were analyzed by ellipsometry in the visible range (430 – 850 nm) in order to determine spectral values of their refractive indices (n, k). A new amorphous dispersion formula was found to accurately describe the optical behavior of SiCNH in the visible range and was used to extrapolate (n,k) in the NIR-IR region. The expected spectral reflectance of the SiCNH materials was calculated from these values, using Fresnel equations which consider optically smooth surfaces. As illustrated in Fig. 2, a good agreement was found between these calculations and the actual reflectance of the films measured by spectrophotometry in the 400 – 1000 nm region. This comparison confirmed the validity of our reflectance calculation and the optical smoothness of the coatings. The choice of the new amorphous dispersion formula to establish SiCNH (n,k) values was also validated. The latter were thus used for multilayer calculation as indicated in the following.

First thermal aging tests were also performed on SiCNH materials. The coatings suffered no alteration of their optical properties after aging under air for 24 h at 450°C. Some coatings underwent rapid thermal annealing (1 min at 800°C) which tended to increase their solar absorption, as indicated by the increase of their absorption index k.

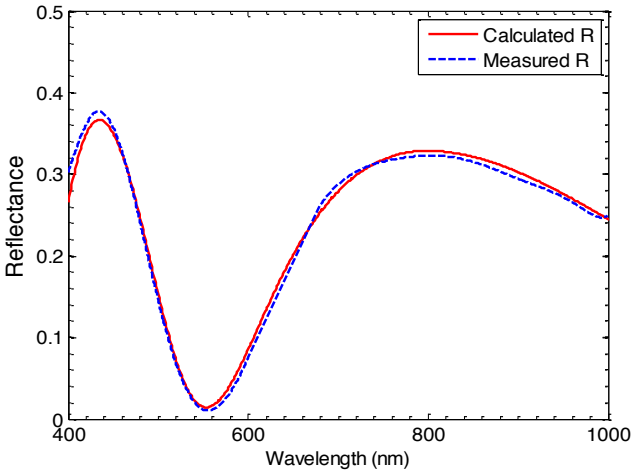

Fig. 2. Comparison of SiCNH reflectances at 10° as measured by spectrophotometry (dotted blue line) and calculated from (n,k) measured by ellipsometry (solid red line).

4.2. Optical modeling of potential SiCNH-based multilayer stacks

Using the refractive indices measured on our SiCNH materials, the optical response of potential multilayer stacks including these materials were simulated in MATLAB and CODE. Reflectance and transmittance of the virtual stacks on stainless steel substrates were calculated. A high refractive index SiCNH material, referred to as $SiCNH_{high}$, was selected as ceramic matrix for W-$SiCNH_{high}$ cermets, which were considered as absorptive layers. Tungsten was chosen because of its high melting point, suitable for high temperature solar applications. As stainless steel is not a good IR reflective metal, the multilayer stacks include tungsten IR reflective layers. A low refraction index SiCNH material, referred to as $SiCNH_{low}$, was selected as antireflective top coating for the multilayers. For each stack, solar absorptance and thermal emittance were deduced from $R(\lambda)$. Thicknesses of the constituting layers, as well as cermet metal volume fractions, were optimized so as to maximize photothermal efficiency $\eta_{photothermal}$, which depends on α_S and ε.

The simulated multilayer stacks are presented in Table 1, along with the corresponding α_S, ε and $\eta_{photothermal}$ at T = 500°C, for two concentration factors (C = 50 and C = 500). Indeed, at higher concentration factors, the influence of α_S becomes preponderant on photothermal efficiency, while that of ε is reduced, as is intuitive from the very definition of $\eta_{photothermal}$. Therefore, for each (C, T) couple depending on the chosen concentrating system and heat transfer fluid, an optimal selective coating exists, which maximizes the radiation-heat conversion efficiency. As an example, a 3-layer and a 6-layer stack are proposed for C = 50 and 500 at T = 500°C (M3-xx and M6-xx). A 5-layer structure was also tested for C = 50 (M5-50), but no 5-layer stack gave a satisfying result for C = 500, therefore the latter case is not reported in Table 1.

The calculated solar absorptance was higher than 0.91 in all cases. One can see that at high concentration factor, the optimization of $\eta_{photothermal}$ allows for ε(500°C) to be higher than at low concentration factor: ε (C = 500) = 0.14-0.20 while ε(C = 50) < 0.08. This flexibility also leads to higher solar absorptance to be reached (up to 0.95), mostly by increasing the cermet tungsten content, up to 26%. The more complex multilayer stacks result in slightly higher efficiencies. Their structure might however be less stable under solar irradiation, due for instance to thermally induced diffusion of the metal. Moreover, the technical difficulty of synthesizing complex multilayers and very thin metal layer might be unacceptable, considering the limited improvement compared to 3-layer structures. The latter seem satisfactory, all the more so as they could be further improved by adding a more efficient antireflective layer.

Table 1. Simulated multilayer stacks and their calculated optical performance: solar absorptance α_S, thermal emittance ε(500°C), photothermal efficiency $\eta_{photothermal}$ for concentration factors C = 50 and C = 500.

Concentration factor **C = 50**	*Multilayer* M3-50	*Multilayer* M5-50	*Multilayer* M6-50
Layer 6			$SiCNH_{low}$ (76 nm)
Layer 5		$SiCNH_{low}$ (58 nm)	W (4 nm)
eLayer 4		$SiCNH_{high}$ (27 nm)	$SiCNH_{high}$ (50 nm)
Layer 3	$SiCNH_{LOW}$ (71 nm)	W (5 nm)	W (10 nm)
Layer 2	20%W-$SiCNH_{high}$ (60 nm)	18%W-$SiCNH_{high}$ (49 nm)	17%W-$SiCNH_{high}$ (52 nm)
Layer 1	W (210 nm)	W (215 nm)	W (225 nm)
Substrate	Stainless steel	Stainless steel	Stainless steel
α_S	0.917	0.913	0.926
ε(500°C)	0.080	0.064	0.076
$\eta_{phototh}$(500°C)	0.879	0.881	0.889

Concentration factor **C = 500**	*Multilayer* M3-500	*Multilayer* M6-500
Layer 6		$SiCNH_{low}$ (80 nm)
Layer 5		W (3 nm)
Layer 4		$SiCNH_{high}$ (53 nm)
Layer 3	$SiCNH_{low}$ (75 nm)	W (4 nm)
Layer 2	26%W-$SiCNH_{high}$ (70 nm)	19%W-$SiCNH_{high}$ (137 nm)
Layer 1	W (192 nm)	W (171 nm)
Substrate	Stainless steel	Stainless steel
α_S	0.930	0.948
ε(500°C)	0.142	0.198
$\eta_{phototh}$(500°C)	0.923	0.938

4.3. Estimated thermo-optical and global efficiencies

The 3-layer stacks (M3-50 and M3-500 in Table 1) were selected to estimate photothermal and global efficiencies as a function of absorber temperature, for a CSP plant using these stacks as solar selective absorber coatings. In a first approach, these results were compared to the ones obtained with a raw steel absorber (α_S = 0.70, ε = 0.80) though existing systems are equipped to ensure a certain amount of spectral selectivity. In the case of central towers, high temperature Pyromark® black paint is usually spread on the steel receiver. It presents high solar absorptivity (α_S = 0.95) but also high emissivity (ε = 0.85), thus limiting the useful power transmitted to the heat transfer fluid. Fresnel linear receivers benefit from the presence of a secondary reflector to increase the amount of absorbed radiation, as well as thermal insulation to reduce thermal losses.

As an example, Fig. 3 represents the calculated photothermal and global efficiencies as a function of absorber temperature, for concentration factors C = 50 (Fresnel and parabolic trough concentrating mirrors) and C = 500 (central towers). When the absorber temperature increases, the photothermal yield decreases because radiative losses

increase with T ($\propto T^4$), as does the thermodynamic efficiency ($\eta_{thermodynamic} \propto -1/T$). Consequently, the system global efficiency presents a maximum at an optimal temperature, which depends on C, α_S and ε. An increase of C or α_S or a decrease of ε lead to increasing $\eta_{photothermal}$, causing the optimal temperature to be shifted towards higher temperatures.

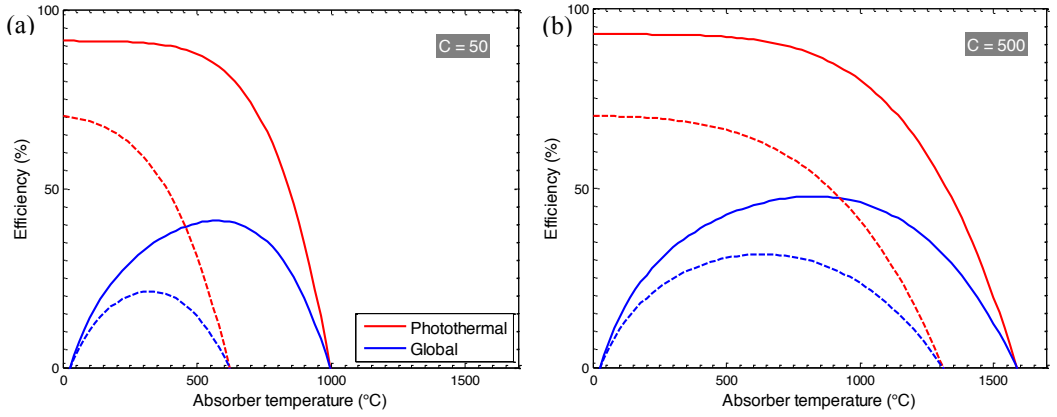

Fig. 3. Photothermal (red) and global (blue) calculated efficiencies as functions of absorber temperature, in the case of a raw steel absorber (dotted lines) and an absorber coated with an optimized 3-layer selective film (solid lines), for concentration factors (a) C = 50 (linear receivers); (b) C = 500 (central towers).

Fresnel reflectors are envisaged for direct steam generation (DSG) systems at temperatures greater than 500°C. For such a concentration system (C = 50) working at T_{abs} = 500°C with superheated steam as the heat transfer fluid, η_{global} was 14% with a raw steel receiver (Fig. 3, dotted line). It rose to 40% with the M3-50 selective coating (180% relative gain) and η_{global} was then maximal between 500 and 650°C. The 3-layer W/SiCNH absorber would therefore be suitable in the case of Fresnel concentrating power plants using superheated steam as the heat transfer fluid (operating $T \geq$ 500°C) and parabolic trough systems working with molten salts ($T \approx$ 560°C).

At a concentration factor C = 500, typical of central towers, the optimal efficiency was reached at approximately 850°C. Selective coatings most likely cannot withstand such temperatures, at least not without losing their spectral selectivity. However, multi-tower systems using molten salts [19] or DSG to operate at temperatures of 500 – 600°C are being developed, and SiCNH absorbers could also provide appropriate selective solutions in such cases. For a central tower (C = 500) working at T_{abs} = 600°C, the global yield rose from 31% for raw steel to 45% when the M3-500 selective coating was used (43% relative gain). If our selective coating is able to sustain 700°C, the global yield would increase from 31 to 47%, i.e. a 50% relative gain.

5. Conclusions

SiCNH films were synthesized by PECVD and characterized so as to investigate their potential as ceramic materials for high temperature solar selective multilayer absorbers. Their complex refractive indices were by ellipsometry to serve as input data for the optical modeling of refractory metal-SiCNH cermets and multilayer stacks. Their reflectance, transmittance, solar absorptance and thermal emittance were calculated. Several multilayer configurations were simulated and optimized in terms of layer thicknesses and compositions so as to maximize their thermo-optical efficiency at a given absorber temperature and concentration factor C. Solar absorptance α_S = 0.92 – 0.95 is expected for multilayer stacks with alternating metal and SiCNH layers. Thermal emittance is expected to be ε(500°C) = 0.06 – 0.08 at low concentration factor (C = 50). The optimization of photothermal efficiency allowed higher ε values at high concentration factor (C = 500), up to 0.20. W/SiCNH-W/SiCNH 3-layer stacks were found to present satisfying optical performance. The corresponding global efficiency at C = 50 was optimal for T = 500 –

650°C (η = 40%). The simulated stacks are therefore suitable as high temperature solar selective absorbers for solar power plants based on linear Fresnel reflectors, parabolic troughs and central tower systems working above 500°C that use molten salts and direct steam generation as heat transfer fluids.

Acknowledgements

This work was supported by the "Laboratory of Excellence" SOLSTICE (Solar Energy: Science, Technology and Innovation for Energy Conversion). The authors are indebted to R. Bazinette and N. Guérin for ellipsometry and spectrophotometry measurements, respectively.

References

[1] Zhang QC, Yin Y, Mills DR. High efficiency Mo-Al_2O_3 cermet selective surfaces for high-temperature application, Sol Energy Mater Sol Cells 1996;40:43-53.
[2] Esposito S, Antonaia A, Addonizio ML, Aprea S. Fabrication and optimisation of highly efficient cermet-based spectrally selective coatings for high operating temperature, Thin Solid Films 2009;517:6000-6.
[3] Antonaia A, Castaldo A, Addonizio ML, Esposito S. Stability of W-Al_2O_3 cermet based solar coating for receiver tube operating at high temperature, Sol Energy Mater Sol Cells 2010;94:1604-11.
[4] Barshilia HC, Selvakumar N, Rajam KS, Sridhara Rao DV, Muraleedharan K. Deposition and characterization of TiAlN/TiAlON/Si_3N_4 tandem absorbers prepared using reactive direct current magnetron sputtering, Thin Solid Films 2008;516:6071-8.
[5] Rebouta L, Pitães A, Andritschky M, Capela P, Cerqueira MF, Matilainen A, Pischow K. Optical characterization of TiAlN/TiAlON/SiO_2 absorber for solar selective applications, Surf. Coat. Technol. 2012;211:41-4.
[6] SunShot Vision Study, Chapter 5: Concentrating Solar Power; Feb 2012.
[7] Soum-Glaude A, Thomas L, Tomasella E. Amorphous silicon carbide coatings grown by low frequency PACVD: Structural and mechanical description, Surf. Coat. Technol. 2006;200:64259.
[8] Schmid U, Eickhoff M, Richter C, Krötz G, Schmitt-Landsiedel D. Etching characteristics and mechanical properties of a-SiC:H thin films, Sens Actuators A 2001;94:87-94.
[9] Zhang F, Xue H, Song Z, Guo Y, Chen G. Effect of high-temperature annealing on the optical-absorption edge of hydrogenated amorphous silicon-carbon films, Phys Rev B 1992;46:4590-4.
[10] Martin I, Vetter M, Orpella A, Puigdollers J, Voz C, Marsal LF, Pallarès J, Alcubilla R. Characterization and application of a-SiC_x:H films for the passivation of the c-Si surface, Thin Solid Films 2002;403-4:476-9.
[11] Kennedy CE, High temperature solar selective coatings, US Patent 2010/0313875 A1; Dec 2010.
[12] Schüler A, Videnovic IR, Oelhafen P, Brunold S. Titanium-containing amorphous hydrogenated silicon carbon films (a-Si:C:H/Ti) for durable solar absorber coatings, Sol Energy Mater Sol Cells 2001;69:271-84.
[13] Forouhi AR, Bloomer I. Optical dispersion relations for amorphous semiconductors and amorphous dielectrics, Phys Rev B 1986;64:7018-26.
[14] Furman ShA, Tikhonrarov AV. Spectral characteristics of multilayer coatings: theory. In: Ed. Frontières. Basics of optics of multilayer systems. Gif-sur-Yvette; 1992.
[15] Palik ED (Ed.). Handbook of Optical Constants of Solids. Boston: Academic Press; 1985.
[16] Bruggeman DAG. Berechnung verschiedener physikalischer Konstanten von heterogenen Substanzen, Ann Phys 1935;24:636-679.
[17] Coating Designer CODE, http://www.wtheiss.com.
[18] Gembicki FW. Vector Optimization for Control with Performance and Parameter Sensitivity Indices. PhD Thesis, Case Western Reserve Univ., Cleveland, Ohio; 1974.
[19] Prosinečki TC, Schnatbaum L. Improvements in solar field layout and molten salt solar tower system design, SolarPACES 2012, Marrakesh, Morocco; 10-14 Sept 2012; heliotower.com.